

# Anthranilic acid analogs as diamagnetic CEST MRI contrast agents that feature an intramolecular-bond shifted hydrogen

Xiaolei Song<sup>a,b†</sup>, Xing Yang<sup>a†</sup>, Sangeeta Ray Banerjee<sup>a</sup>,  
Martin G. Pomper<sup>a\*</sup> and Michael T. McMahon<sup>a,b\*</sup>



Diamagnetic chemical exchange saturation transfer (diaCEST) agents are a new class of imaging agents, which have unique magnetic resonance (MR) properties similar to agents used for optical imaging. Here we present a series of anthranilic acid analogs as examples of diaCEST agents that feature an exchangeable proton shifted downfield, namely, an intramolecular-bond shifted hydrogen (IM-SHY), which produces significant and tunable contrast at frequencies of 4.8–9.3 ppm from water. Five analogs of *N*-sulfonyl anthranilic acids are all highly soluble and produced similar CEST contrast at ~6–8 ppm. We also discovered that flufenamic acid, a commercial nonsteroidal anti-inflammatory drug, displayed CEST contrast at 4.8 ppm. For these N–H IM-SHY agents, the contrast produced was insensitive to pH, making them complementary to existing diaCEST probes. This initial IM-SHY library includes the largest reported shifts for N–H protons on small organic diaCEST agents, and should find use as multifrequency MR agents for *in vivo* applications. Copyright © 2014 John Wiley & Sons, Ltd.

Additional supporting information may be found in the online version of this article at the publisher's web site.

**Keywords:** chemical exchange saturation transfer; *N*-sulfonyl anthranilic acid derivatives; molecular imaging; *N*-aryl anthranilic acid derivatives

## 1. INTRODUCTION

Chemical exchange saturation transfer (CEST) contrast agents, first introduced in 2000 (1), are an alternative to traditional magnetic resonance (MR) contrast agents, which rely on direct enhancement of water relaxivity. The CEST mechanism involves saturation of labile protons on the agents via selective irradiation at their resonance frequencies. The signal loss is then transferred to surrounding bulk water through chemical exchange, leading to a reduction in water signal (2–4). This water signal loss (CEST contrast) results in an amplification of the signal from low-concentration protons through the multiple exchange events occurring during the saturation pulse. Because the CEST contrast is derived from irradiation at a specific proton frequency, it is easier to discriminate from other sources of signal change than  $T_1$  or  $T_2^*$  contrast. This frequency dependence of contrast also allows the simultaneous detection and discrimination of multiple agents within an image (5–7). Diamagnetic CEST (diaCEST) and paramagnetic CEST (paraCEST) agents have been the subjects of several recent reviews (8–11). DiaCEST agents, such as glucose (12–14), glycogen (15), *myo*-inositol (16), glutamate (17), creatine (18,19), *L*-arginine (20,21), glycosaminoglycans (22,23) and peptides (5,24–26), are attractive biocompatible materials, but compared with paraCEST agents (27), they suffer from reduced sensitivity owing to the relatively small chemical shift difference between their exchangeable protons and those of water (1–5.0 ppm). To address this issue, diaCEST agents with protons of increased chemical shift have been reported, including the thymidine analogs (5.5 ppm) (28) and iopamidol (4.2 and 5.5 ppm) (29,30). Most recently, we reported that the C2–OH in 2-hydroxybenzoic acid analogs

resonates between 8.7 and 10.8 ppm from water, with solute-to-water exchange rates ( $k_{sw}$ ) that are well suited to CEST imaging (31). Building upon that report, here we describe the anthranilic acid analogs: *N*-aryl derivatives, *N*-acyl derivatives and *N*-sulfonyl derivatives, as another class of IntraMolecular-Bond Shifted Hydrogens exchangeable proton (IM-SHY) diaCEST agents, based on the exchange of N–H protons instead of O–H (Scheme 1).

## 2. RESULTS AND DISCUSSION

Salicylic acid (1) displays CEST contrast at 9.3 ppm (31) (Fig. 1). This dramatic chemical shift derives from the low barrier

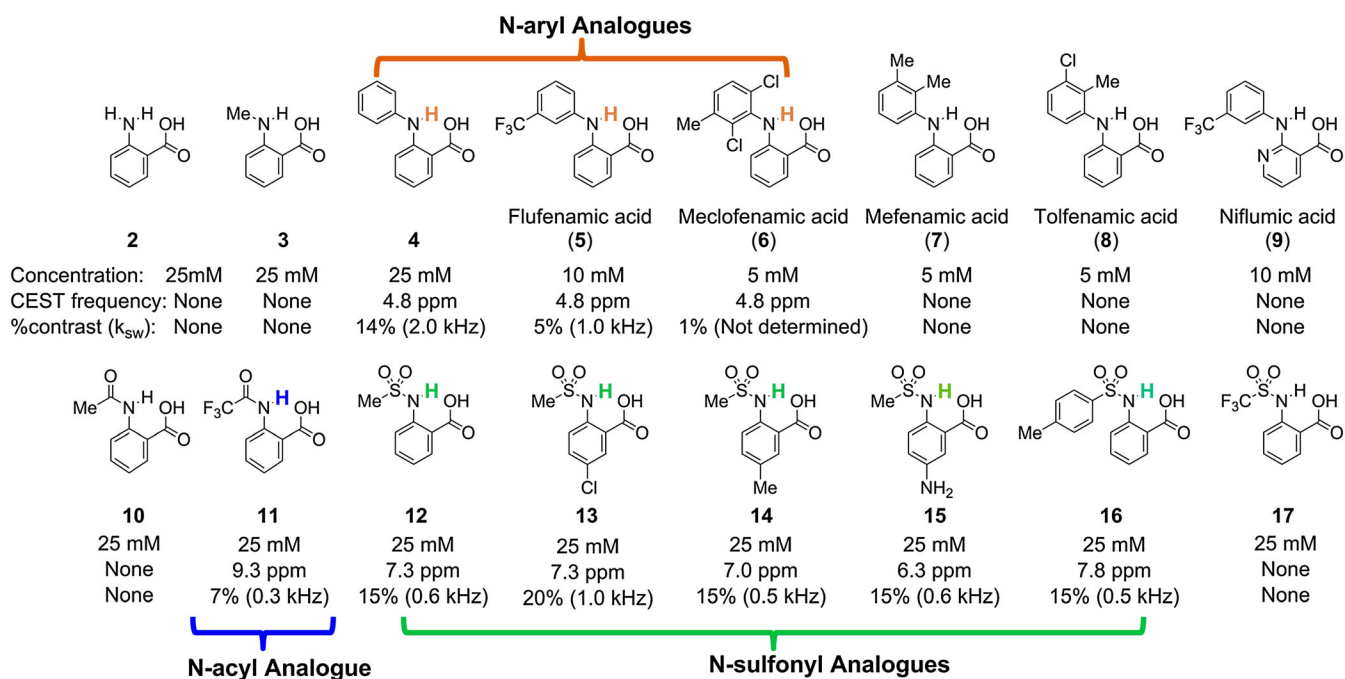
\* Correspondence to: M. T. McMahon, F.M. Kirby Research Center for Functional Brain Imaging, Kennedy Krieger Institute, 707 N. Broadway, Baltimore, MD 21287, USA. E-mail: mcmahon@mri.jhu.edu

M. G. Pomper, Russell H. Morgan Department of Radiology and Radiological Science, Baltimore, MD 21287, USA. E-mail: mpomper@jhmi.edu

† Xiaolei Song and Xing Yang contributed equally to this work.

a X. Song, X. Yang, S. Ray Banerjee, M. G. Pomper, M. T. McMahon  
Russell H. Morgan Department of Radiology and Radiological Science, The Johns Hopkins University School of Medicine, Baltimore, Maryland, USA

b X. Song, M. T. McMahon  
F.M. Kirby Research Center for Functional Brain Imaging, Kennedy Krieger Institute, Baltimore, Maryland, USA



**Scheme 1.** Chemical exchange saturation transfer (CEST) frequency (ppm), contrast (%) and  $k_{sw}$  (kHz) of anthranilic acid and its analogs. Experimental conditions: pH 7.1–7.5, using  $T_{sat} = 3$  s,  $B_1 = 3.6$   $\mu$ T. For Z-spectra, see Tables S1 and S2 in the Supporting Information. All the MR experiments were performed at 37 °C.

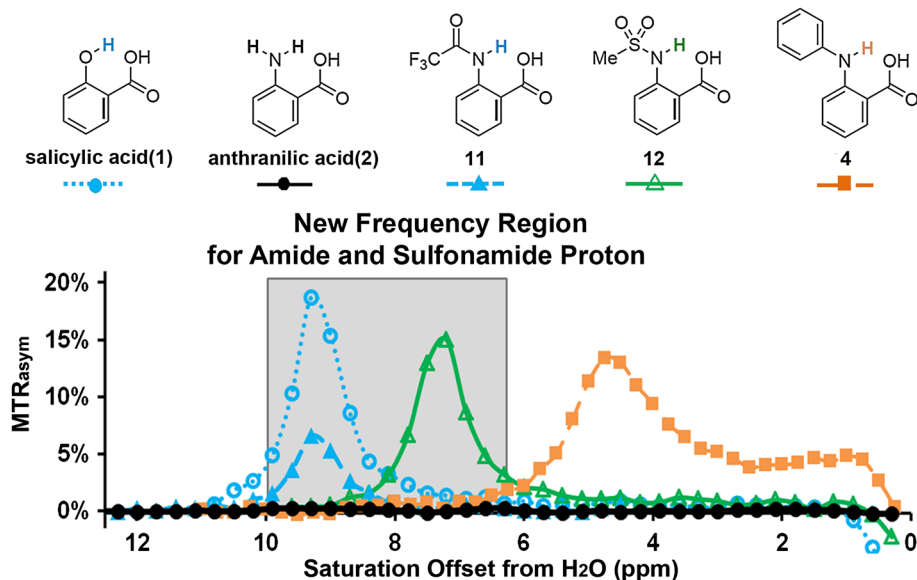


**Figure 1.** CEST contrast curves for representative salicylic acid (1) and anthranilic acid derivatives (2, 4, 11 and 12) at concentrations of 25 mM (pH 7.1–7.4) using  $B_1 = 3.6$   $\mu$ T,  $T_{sat} = 3$  s. The gray box indicates this group of agents includes a new frequency region for amide and sulfonamide protons.

hydrogen bond between the exchangeable phenolic proton and the carboxylate anion at neutral pH (32,33). We also determined that similar CEST signals could be observed in other compounds with the 2-hydroxybenzoic acid scaffold, representing a powerful new type of CEST agent, based on the principle of IM-SHY (31). We were interested in preparing similar agents with labile anthranilic rather than phenolic protons to explore further the capabilities of the benzoic acid core for generating CEST contrast. However, anthranilic acid (2), an N–H analog of salicylic acid, failed to produce contrast (Scheme 1, Fig. 1). To understand why, we measured the CEST contrast properties of a wide range of common anthranilic acid analogs, including those

with *N*-alkyl, *N*-aryl, *N*-acyl and *N*-sulfonyl substitutions (Scheme 1). Interestingly, significant contrast was observed in *N*-phenylanthranilic acid (4), although the labile protons resonate at 4.8 ppm, which is much lower than the 9.3 ppm observed in 1. At a relatively low saturation field strength ( $B_1 = 3.6$   $\mu$ T), 4 showed a broader peak in the CEST spectrum than 1 and 12 (Fig. 1b), indicating a faster exchange. Using the QUESP (QUantifying Exchange rates using Saturation Power dependence) experiment (34) we measured  $k_{sw} = 2.0$  kHz (Supporting Information, Fig. S1), which is slightly too fast to obtain optimal CEST contrast using the 3–5  $\mu$ T saturation pulses we are able to employ on our clinical scanners. Comparing the CEST signal between 4 and 2, the loss

of CEST signal in **2** indicates that  $k_{sw}$  is too high. This is possibly due to the presence of the additional nonhydrogen-bonded C2 N-H proton, which might undergo a fast intramolecular exchange with the hydrogen-bonded proton. In addition, if we modify **2** through substitution of a methyl group for one of the amine protons (**3**), the CEST contrast is still absent, which implies that stereoelectronic influences are also important (Scheme 1). It is worth mentioning that *N*-phenylanthranilic acid analogs are commonly used as nonsteroidal anti-inflammatory drugs. The CEST properties were measured on five commercially available drugs: flufenamic acid (**5**), meclofenamic acid (**6**), mefenamic acid (**7**), tolfenamic acid (**8**) and niflumic acid (**9**). Their water solubility is generally low (~10 mM or lower). As shown in Scheme 1, flufenamic acid (**5**) showed similar CEST properties to **4**. The exchangeable proton resonates at 4.8 ppm, with  $k_{sw} = 1.0$  kHz. The CEST data of **6–8** indicated the importance of steric interaction on the proton exchange rate with water. Adding the chloro group ortho to the exchangeable N-H (**6**) reduced its water accessibility and the CEST contrast dropped to 1%. This is presumably because the exchange is too slow; however, it is difficult to quantify  $k_{sw}$  because of the small contrast. Increasing the steric hindrance through addition of methyl (**7** and **8**) eliminated the CEST signal. Niflumic acid (**9**), the pyridine analog of **5**, did not display any CEST contrast. One possible explanation is that the presence of the pyridine nitrogen tends to strongly hydrogen bond to water and alters the proton exchange of the IM-SHY -NH.

We next determined the detection limits of **5** with CEST, because it could potentially be translated into clinical applications (35). The solubility of **5** is quite poor at pH values below 7; however, 10 mM could be achieved in phosphate-buffered saline buffer at pH above 7.2. As shown by the QUESP data in Fig. 2 (a), the contrast is near maximal at  $B_1 > 6$   $\mu$ T, with a smaller  $k_{sw}$  (1.0 kHz) than that of **4**. The peaks in the Z-spectrum and the  $MTR_{asym}$  spectrum are also sharper than those of **4** (Table S1), which is also due to a slower  $k_{sw}$ . The contrast of **5** is nearly linearly dependent with concentration over a range from 0.75 to 10 mM (36) (pH 7.4), with 1.2% contrast observed at a concentration of 1.5 mM (Fig. 2b).

In an attempt to increase the chemical shift further to fit the slow to intermediate detection window of CEST ( $k_{sw} < \Delta\omega$ ) while still keeping  $k_{sw}$  slow enough to achieve efficient saturation using a  $B_1$  suitable for the MR hardware used in our *in vivo* scans, we investigated the C2 amide analogs of anthranilic acid. Amide N-H protons tend to be shifted further than amine protons,

although they also tend to exchange with water more slowly as well (**5**). As expected, **10** did not show any CEST contrast, presumably because the  $k_{sw}$  is too slow (Fig. 3a, Scheme 1). However, after modification of the structure to **11**, an example of a more acidic N-H proton, we observed CEST contrast with the labile proton resonating at 9.3 ppm, indicating a strong hydrogen bond interaction in water. The contrast produced by **11** is relatively low (6% at 25 mM,  $B_1 = 3.6$   $\mu$ T), because  $k_{sw}$  is relatively slow (0.3 kHz, see Supporting Information, Figs S2 and S3 for QUESP/pH details). Further increasing the acidity through 2-(methyl-sulfonamido) benzoic acid (**12**) resulted in more substantial contrast at 7.3 ppm (~15% at 25 mM,  $B_1 = 3.6$   $\mu$ T), based on adjusting the proton exchange of the IM-SHY-NH. According to our QUESP measurements, **12** displays a  $k_{sw} = 0.6$  kHz at pH = 7.1, which is quite similar to salicylic acid (**31**) and barbituric acid (Supporting Information, Fig. S5). Maximum contrast was achieved using  $B_1 = 6$   $\mu$ T or higher with ~90% of this contrast available at  $B_1 = 3.6$   $\mu$ T (Fig. 3c), which is near the maximum power we can apply using a parallel transmit body coil on our clinical scanners. More interestingly, the contrast and  $k_{sw}$  of **11** and **12** remained almost constant between the pH values 6 and 8 (Figs 3d and Figs S2–S4 in the Supporting Information). For comparison, salicylic acid (**1**), an alternative IM-SHY agent, possesses protons with  $k_{sw}$  that decrease dramatically over this range ( $k_{sw} = 2.4$  kHz at pH 6.5,  $k_{sw} = 0.4$  kHz at pH 7.8). This pH independence makes **11** and **12** ideal IM-SHY probes for *in vivo* quantification purposes. As expected, a nearly linear relationship between contrast and concentration was observed for **12** (Fig. 3b), with 1% CEST contrast produced at a concentration of 1.5 mM. Although the chemical shift is not as large as **1** or **11**, **12** represents the first diaCEST agent with labile N-H protons resonating at 7–8 ppm from water that produces significant contrast. This compound should be useful for multiple frequency detection and complementary to other existing diaCEST probes.

Encouraged by the result from **12**, we studied several commercially available analogs to check if the CEST contrast of this scaffold would tolerate chemical modification. As shown in Scheme 1 and Fig. 3(e), similar contrast was obtained upon chemical modification of the aniline ring (**13–15**), with the CEST frequency varying from 6 to 7.3 ppm. Placing a strong electron donating -NH<sub>2</sub> group (**15**) at the *para*-position to the C2-NH reduced the CEST frequency to 6.3 ppm, which is quite similar to the electronic effects we observed previously (**31**). Placing a -Cl at the *para*-position of the C2-NH (**13**) led to faster  $k_{sw}$

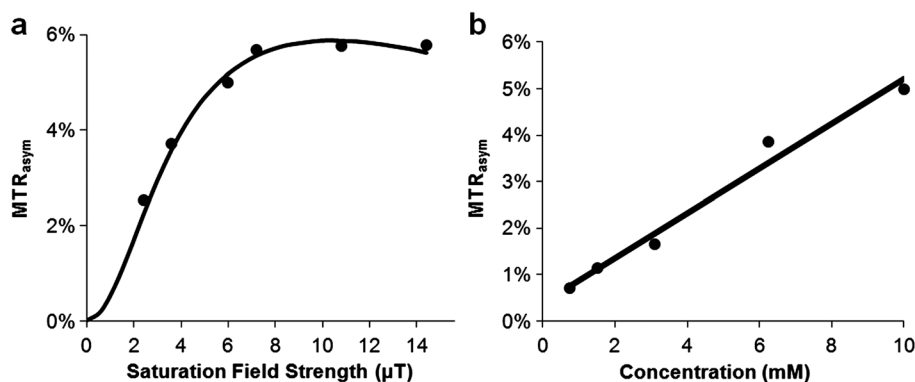


**Figure 2.** CEST properties of **5**. (a) QUESP data at 10 mM at pH = 7.4, with  $k_{sw} = 1.0$  kHz where the data are shown as points and the solid line represents the best fit after numerically solving the two-pool Bloch equations; (b) CEST contrast at 4.8 ppm as a function of concentration using  $B_1 = 3.6$   $\mu$ T (solid line: linear fitting).

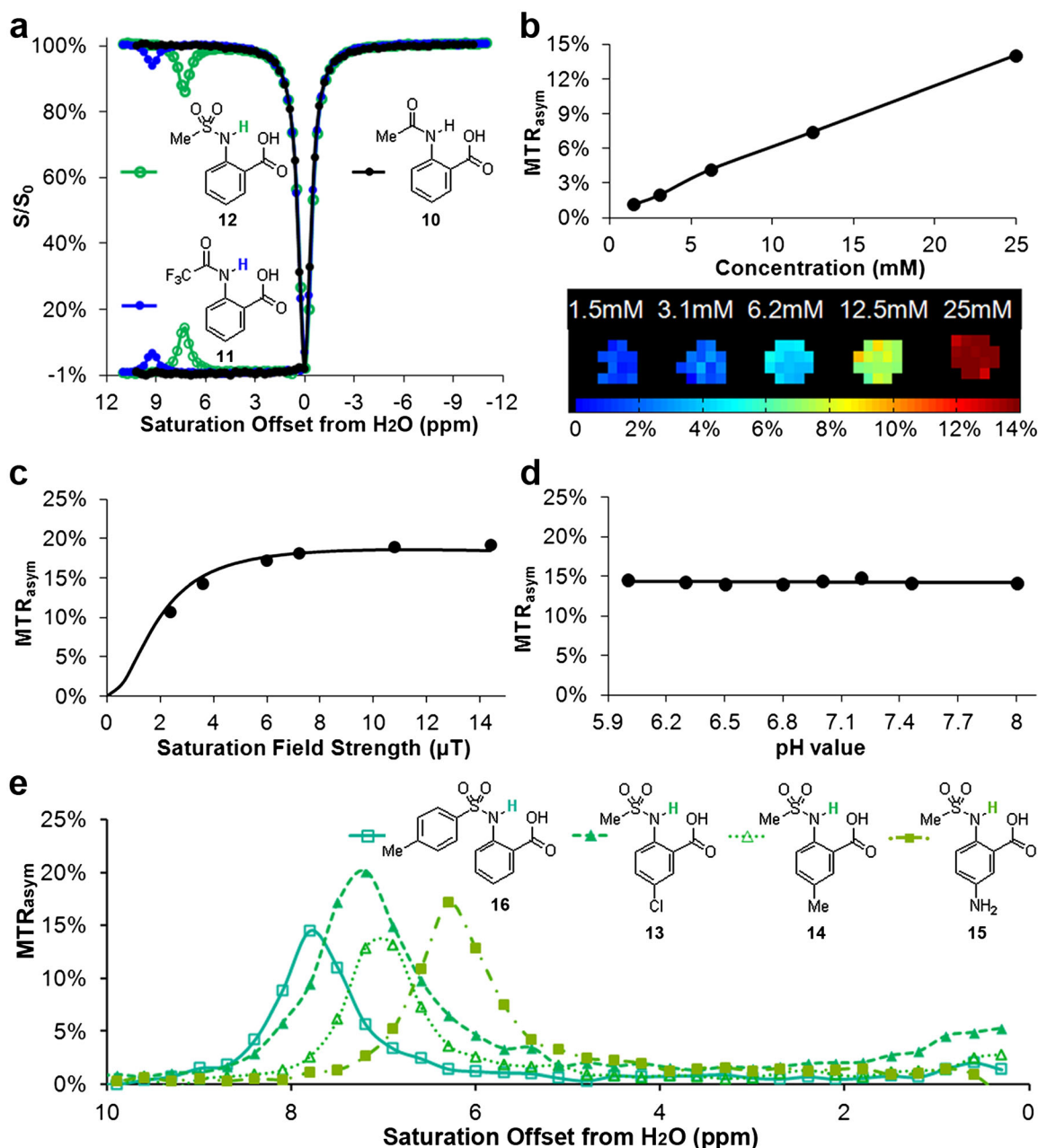


**Figure 3.** CEST properties of **10–16**. (a) Z-spectra and MTR<sub>asym</sub> for **10–12** at 25 mM, pH = 7.2,  $T_{\text{sat}} = 3$  s and  $B_1 = 3.6$   $\mu\text{T}$ ; (b) CEST contrast of **12** at 7.5 ppm as a function of concentration, using  $B_1 = 3.6$   $\mu\text{T}$ ; (c) QUESP data of **12** at 25 mM, pH = 7.1, with  $k_{\text{sw}} = 0.6$  kHz; (d) pH dependence of percentage contrast for **12**; and (e) analogs of **12** with different CEST peak frequencies from 6 to 8 ppm.

(1.0 kHz), and as a result a higher CEST contrast (~20%). Substitution of a phenyl for the methyl (**16**) resulted in deshielding with the chemical shift increased to 7.8 ppm. In comparison, replacing the methyl group in **12** with a  $-\text{CF}_3$  (**17**) resulted in loss of CEST contrast. As this group of agents, **12–16**, generated similar contrast to **1** in phantoms, we further chose to monitor *in vivo* the contrast in kidneys after administration into the tail vein of mice of the most sensitive, **13** (Fig. 4). The contrast was monitored over time, and compared with the pre-injection images (Fig. 4b); we observed a 2–3% increase in the CEST contrast 7.5 min after injection integrating from 7.0 to 7.6 ppm (Fig. 4b, c). The histogram in Fig. 4(d) indicates the pixelwise distribution of MTR<sub>asym</sub> values for mouse 1 pre- and post-injection. A negative MTR<sub>asym</sub> was

observed as baseline for the kidneys, which is presumably due to strong relayed NOE transfer of signal loss to water (37,38). As shown in Fig. 4(e), for both mice the contrast reached maximum at ~7.5 min post-injection

As shown above, anthranilic acid IM-SHY probes have larger shifts for their exchangeable protons than spherical lipoCEST agents (**10**), and similar shifts to those found for paraCEST probes such as Yb-DO3A-oAA (39). The shifts are not nearly as large as some of the Yb, Eu, Tm or Dy complexes described previously (40–43) or the cryptophane cages used for hyperCEST (43); however, because  $k_{\text{sw}}$  can be tuned to be as slow as 0.5–1 kHz through structure changes and is insensitive to pH in the physiologically relevant range, these IM-SHY probes are well suited for detection using saturation pulses attainable on clinical scanners.

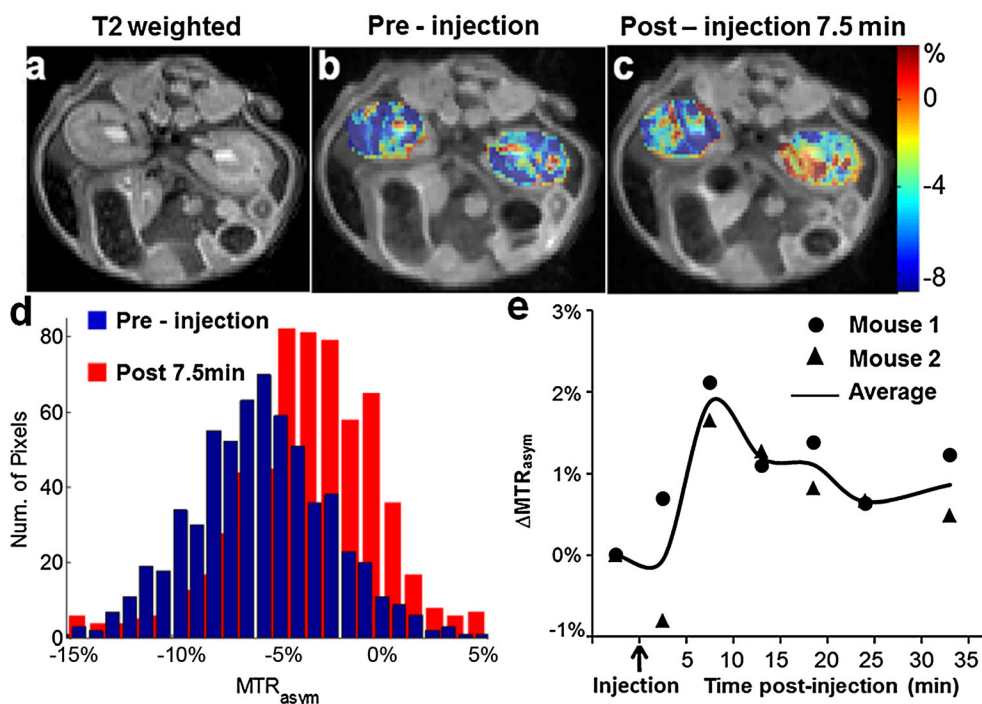


**Figure 4.** *In vivo* contrast for **13**. (a)  $T_{2w}$  image; (b) overlay  $MTR_{asymp}$  map pre-injection for mouse 1; (c) overlay  $MTR_{asymp}$  map at 10 min post-injection for mouse 1; (d) histogram displaying the distribution of  $MTR_{asymp}$  for mouse 1 pre- and post-injection (c, d). (e) Dynamic time course of  $\Delta MTR_{asymp}$  based on regions of interest enclosing both left and right kidneys for the two mice using  $\omega_1 = 3.6 \mu\text{T}$  (circle: mouse 1; triangle: mouse 2; solid line, average value of mouse 1 and mouse 2).

A more detailed investigation of the steric and electronic factors for this scaffold is ongoing.

### 3. CONCLUSION

We have demonstrated that anthranilic acid provides a suitable scaffold for tunable IM-SHY diaCEST agents. Labile protons in *N*-aryl anthranilic acids (**4–6**) resonate at 4.8 ppm while for *N*-sulfonyl anthranilic acids (**12–16**) these resonate between 6 and 8 ppm and for **11** labile protons resonate at 9.3 ppm. Anthranilic acid analogs could be used for multicolor MR imaging, with one nonsteroidal anti-inflammatory drug, **5**, already administered to patients, having been identified among these analogs. The 2-sulfonamidobenzoic acid scaffold has been shown to allow chemical modification with labile protons that exchange in a non-pH-dependent manner, which could be advantageous for *in vivo* quantification. Additional studies are ongoing to improve our understanding of the relationship between CEST properties and molecular structure for these and other IM-SHY diaCEST agents.

## 4. EXPERIMENTAL SECTION

### 4.1. Phantom Preparation and Data Acquisition

Compounds **1–12** were purchased from Sigma Aldrich (St Louis, MO, USA). Compounds **13–17** were purchased from Enamine Ltd (Monmouth, NJ, USA). Samples were dissolved in 0.01 M phosphate-buffered saline at several concentrations from 1.5 to 25 mM depending on the solubility, and titrated using high-concentration HCl/NaOH to various pH values ranging from 6 to 8. The solutions were placed into 1 mm glass capillaries and assembled in a holder for CEST MR imaging. They were kept at 37°C during imaging. Phantom CEST experiments were performed

on a Bruker 11.7 T vertical bore MR scanner, using a 20 mm birdcage transmit/receive coil. CEST images were acquired using a Rapid Acquisition with Refocused Echoes (RARE) (RARE factor = 8) sequence with a continuous wave saturation pulse length of 3 s and saturation field strength ( $B_1$ ) from 1.2 to 14.4  $\mu\text{T}$ . The CEST Z-spectra were acquired by incrementing the saturation frequency every 0.3 ppm from  $-15$  to 15 ppm; repetition time ( $TR$ )/effective echo time ( $TE$ ) = 6 s/17 ms with linear phase-encoding, matrix size =  $64 \times 48$  and slice thickness = 1.2 mm. For determining  $k_{sw}$  using QUESP, Z-spectra were collected at  $B_1 = 1.2, 2.4, 3.6, 5.4, 7.2, 10.8$  and 11.4  $\mu\text{T}$ .

### 4.2. In Vivo Mouse Imaging

To evaluate whether the *N*-sulfonyl derivatives, **12–16**, could be detected after administration into live animals, we injected two mice with 60  $\mu\text{L}$  of a 0.25 M solution of compound **13** and collected CEST images. Images consisting of a single axial slice containing both kidneys were collected. To improve the temporal resolution and able to correct the  $B_0$  shift, we collected a partial Z-spectrum every 5 min by incrementing  $\Delta\omega$  over 10 frequencies ( $\pm 8.2, \pm 7.6, \pm 7.3, \pm 7$  and  $\pm 6.6$  ppm), and an average  $MTR_{asymp}$  (at  $\pm 7.6, \pm 7.3$  and  $\pm 7$  ppm). The imaging sequence employed is the same as for the phantoms, with the following parameters:  $B_1 = 3.6 \mu\text{T}$ , saturation duration ( $T_{sat}$ ) 3 s,  $TR$ /effective  $TE = 5$  s/16 ms with linear phase-encoding, matrix size  $96 \times 64$ .

### 4.3. Post-processing

CEST contrast was quantified using  $MTR_{asymp} = [S(-\Delta\omega) - S(+\Delta\omega)]/S_0$  for phantom and  $1 - S(+\Delta\omega)/S(-\Delta\omega)$  *in vivo* to increase the temporal resolution and reduce the motion where  $S(+\Delta\omega)$  represents water signal intensity with a saturation pulse applied at the frequency  $+\Delta\omega$  and  $S_0$  represents the water signal without a saturation pulse.

The Z-spectra were corrected pixel by pixel using a  $B_0$  map acquired using Water Saturation Shift Referencin (WASSR) as described in detail previously (9). To indicate the kinetics of CEST contrast upon injection of the agents, we subtracted the  $MTR_{\text{asym}}$  values at each time-point with a reference  $MTR_{\text{asym}}(0)$ , and plotted the averaged  $\Delta MTR_{\text{asym}}(t) = MTR_{\text{asym}}(t) - MTR_{\text{asym}}(0)$ , and plotted the averaged  $\Delta MTR_{\text{asym}}(t)$  of the whole kidney as a function of minutes post-injection. The solvent to water exchange rate ( $k_{\text{sw}}$ ) was calculated according to the QUEST and/or QUESP methods (34), which were considered as a simple and robust method for estimating  $k_{\text{sw}}$ , especially for the slow to intermediate exchange regime (44,45). In particular we numerically solved the two-pool model Bloch equations to fit the measured  $MTR_{\text{asym}}$  values as a function of different  $T_{\text{sat}}$  or  $B_1$  as described previously (34), with the following relaxation parameters for water and solute respectively, where  $R_{1w}$  is the longitudinal relaxation time for water and  $R_{2w}$  is the transverse relaxation time for water:  $R_{2w} = 0.9 \text{ s}^{-1}$ ,  $R_{1s} = 0.71 \text{ s}^{-1}$ ,  $R_{2s} = 39 \text{ s}^{-1}$ .  $R_{1w}$  was allowed to float between 0.33 and  $0.40 \text{ s}^{-1}$  to obtain the best fit. The QUESP/QUEST fittings are shown in the Supporting Information, Figs S1–S5.

## REFERENCES

- Ward KM, Aletras AH, Balaban RS. A new class of contrast agents for MRI based on proton chemical exchange dependent saturation transfer (CEST). *J Magn Reson* 2000; 143(1): 79–87.
- Aime S, Delli Castelli D, Terreno E. Novel pH-reporter MRI contrast agents. *Angew Chem* 2002; 114(22): 4510–4512.
- Ward KM, Balaban RS. Determination of pH using water protons and chemical exchange dependent saturation transfer (CEST). *Magn Reson Med* 2000; 44(5): 799–802.
- De Leon-Rodriguez LM, Lubag AJM, Malloy CR, Martinez GV, Gillies RJ, Sherry AD. Responsive MRI agents for sensing metabolism in vivo. *Acc Chem Res* 2009; 42(7): 948–957.
- McMahon MT, Gilad AA, DeLiso MA, Berman SM, Bulte JW, van Zijl PC. New 'multicolor' polypeptide diamagnetic chemical exchange saturation transfer (DIACEST) contrast agents for MRI. *Magn Reson Med* 2008; 60(4): 803–812.
- Aime S, Carrera C, Delli Castelli D, Geninatti C, Terreno E. Tunable imaging of cells labeled with MRI-PARACEST agents. *Angew Chem Int Edn* 2005; 44(12): 1813–1815.
- Viswanathan S, Ratnakar SJ, Green KN, Kovacs Z, De Leon-Rodriguez LM, Sherry AD. Multi-frequency PARACEST agents based on europium(III)-DOTA-tetraamide ligands. *Angew Chem* 2009; 48(49): 9330–9333.
- van Zijl PC, Yadav NN. Chemical exchange saturation transfer (CEST): what is in a name and what isn't? *Magn Reson Med* 2011; 65(4): 927–948.
- Liu G, Song X, Chan KW, McMahon MT. Nuts and bolts of chemical exchange saturation transfer MRI. *NMR Biomed* 2013; 26(7): 810–828.
- Castelli DD, Terreno E, Longo D, Aime S. Nanoparticle-based chemical exchange saturation transfer (CEST) agents. *NMR Biomed* 2013; 26(7): 839–849.
- Soesbe TC, Wu Y, Dean Sherry A. Advantages of paramagnetic chemical exchange saturation transfer (CEST) complexes having slow to intermediate water exchange properties as responsive MRI agents. *NMR Biomed* 2013; 26(7): 829–838.
- Chan KW, McMahon MT, Kato Y, Liu G, Bulte JW, Bhujwalla ZM, Artemov D, van Zijl PC. Natural D-glucose as a biodegradable MRI contrast agent for detecting cancer. *Magn Reson Med* 2012; 68(6): 1764–1773.
- Walker-Samuel S, Ramasawmy R, Torrealdea F, Rega M, Rajkumar V, Johnson SP, Richardson S, Goncalves M, Parkes HG, Arstad E, Thomas DL, Pedley RB, Lythgoe MF, Golay X. In vivo imaging of glucose uptake and metabolism in tumors. *Nat Med* 2013; 19(18): 1067–1072.
- Jin T, Autio J, Obata T, Kim S-G. Spin-locking versus chemical exchange saturation transfer MRI for investigating chemical exchange process between water and labile metabolite protons. *Magn Reson Med* 2011; 65(5): 1448–1460.
- van Zijl PC, Jones CK, Ren J, Malloy CR, Sherry AD. MRI detection of glycogen in vivo by using chemical exchange saturation transfer imaging (glycoCEST). *Proc Natl Acad Sci USA* 2007; 104(11): 4359–4364.
- Haris M, Cai K, Singh A, Hariharan H, Reddy R. In vivo mapping of brain myo-inositol. *Neuroimage* 2011; 54(3): 2079–2085.
- Cai K, Haris M, Singh A, Kogan F, Greenberg JH, Hariharan H, Detre JA, Reddy R. Magnetic resonance imaging of glutamate. *Nat Med* 2012; 18(2): 302–306.
- Haris M, Nanga RP, Singh A, Cai K, Kogan F, Hariharan H, Reddy R. Exchange rates of creatine kinase metabolites: feasibility of imaging creatine by chemical exchange saturation transfer MRI. *NMR Biomed* 2012; 25(11): 1305–1309.
- Kogan F, Haris M, Singh A, Cai K, Debrosse C, Nanga RP, Hariharan H, Reddy R. Method for high-resolution imaging of creatine in vivo using chemical exchange saturation transfer. *Magn Reson Med* 2013.
- Chan KW, Liu G, Song X, Kim H, Yu T, Arifin DR, Gilad AA, Hanes J, Walczak P, van Zijl PC, Bulte JW, McMahon MT. MRI-detectable pH nanosensors incorporated into hydrogels for in vivo sensing of transplanted-cell viability. *Nat Mater* 2013; 12(3): 268–275.
- Liu G, Moake M, Har-el YE, Long CM, Chan KW, Cardona A, Jamil M, Walczak P, Gilad AA, Sgouros G, van Zijl PC, Bulte JW, McMahon MT. In vivo multicolor molecular MR imaging using diamagnetic chemical exchange saturation transfer liposomes. *Magn Reson Med* 2012; 67(4): 1106–1113.
- Saar G, Zhang B, Ling W, Regatte RR, Navon G, Jerschow A. Assessment of glycosaminoglycan concentration changes in the intervertebral disc via chemical exchange saturation transfer. *NMR Biomed* 2012; 25(2): 255–261.
- Ling W, Regatte RR, Navon G, Jerschow A. Assessment of glycosaminoglycan concentration in vivo by chemical exchange-dependent saturation transfer (gagCEST). *Proc Natl Acad Sci USA* 2008; 105(7): 2266–2270.
- Gilad AA, McMahon MT, Walczak P, Winnard PT Jr, Raman V, van Laarhoven HW, Skoglund CM, Bulte JW, van Zijl PC. Artificial reporter gene providing MRI contrast based on proton exchange. *Nat Biotechnol* 2007; 25(2): 217–219.
- Zhou J, Lal B, Wilson DA, Larterra J, van Zijl PC. Amide proton transfer (APT) contrast for imaging of brain tumors. *Magn Reson Med* 2003; 50(6): 1120–1126.
- Airan RD, Bar-Shir A, Liu G, Pelled G, McMahon MT, van Zijl PC, Bulte JW, Gilad AA. MRI biosensor for protein kinase A encoded by a single synthetic gene. *Magn Reson Med* 2012; 68(6): 1919–1923.
- Hancu I, Dixon WT, Woods M, Vinogradov E, Sherry AD, Lenkinski RE. CEST and PARACEST MR contrast agents. *Acta Radiol* 2010; 51(8): 910–923.
- Bar-Shir A, Liu G, Liang Y, Yadav NN, McMahon MT, Walczak P, Nimmagadda S, Pomper MG, Tallman KA, Greenberg MM, van Zijl PC, Bulte JW, Gilad AA. Transforming thymidine into a magnetic resonance imaging probe for monitoring gene expression. *J Am Chem Soc* 2013; 135(4): 1617–1624.
- Aime S, Calabi L, Biondi L, De Miranda M, Ghelli S, Paleari L, Rebaudengo C, Terreno E. Iopamidol: Exploring the potential use of a well-established X-ray contrast agent for MRI. *Magn Reson Med* 2005; 53(4): 830–834.
- Longo DL, Dastru W, Digilio G, Keupp J, Langereis S, Lanzardo S, Prestigio S, Steinbach O, Terreno E, Uggeri F, Aime S. Iopamidol as a responsive MRI-chemical exchange saturation transfer contrast agent for pH mapping of kidneys: in vivo studies in mice at 7 T. *Magn Reson Med* 2011; 65(1): 202–211.
- Yang X, Song X, Li Y, Liu G, Ray Banerjee S, Pomper MG, McMahon MT. Salicylic acid and analogs: diamagnetic chemical exchange saturation transfer (diaCEST) magnetic resonance imaging (MRI) contrast agents with highly shifted exchangeable protons. *Angew Chemie Int Edn* 2013; 52(31): 8116–8119.
- Maciel GE, Savitsky GB. Carbon-13 chemical shifts + intramolecular hydrogen bonding. *J Phys Chem* 1964; 68(2): 437.
- Mock WL, Morsch LA. Low barrier hydrogen bonds within salicylate mono-anions. *Tetrahedron* 2001; 57(15): 2957–2964.
- McMahon MT, Gilad AA, Zhou J, Sun PZ, Bulte JW, van Zijl PC. Quantifying exchange rates in chemical exchange saturation transfer agents using the saturation time and saturation power dependencies of the magnetization transfer effect on the magnetic resonance imaging signal (QUEST and QUESP): Ph calibration for poly-L-lysine and a starburst dendrimer. *Magn Reson Med* 2006; 55(4): 836–847.
- Lovering AL, Ride JP, Bunce CM, Desmond JC, Cummings SM, White SA. Crystal structures of prostaglandin D-2 11-ketoreductase (AKR1C3) in complex with the nonsteroidal anti-inflammatory drugs flufenamic acid and indomethacin. *Cancer Res* 2004; 64(5): 1802–1810.

36. Ali MM, Liu G, Shah T, Flask CA, Pagel MD. Using two chemical exchange saturation transfer magnetic resonance imaging contrast agents for molecular imaging studies. *Acc Chem Res* 2009; 42(7): 915–924.
37. Jones CK, Huang A, Xu J, Edden RA, Schar M, Hua J, Oskolkov N, Zaca D, Zhou J, McMahon MT, Pillai JJ, van Zijl PC. Nuclear Overhauser enhancement (NOE) imaging in the human brain at 7T. *Neuroimage* 2013; 77: 114–124.
38. Pekar J, Jezzard P, Roberts DA, Leigh JS, Jr., Frank JA, McLaughlin AC. Perfusion imaging with compensation for asymmetric magnetization transfer effects. *Magn Reson Med* 1996; 35(1): 70–79.
39. Liu GS, Li YG, Sheth VR, Pagel MD. Imaging in vivo extracellular pH with a single paramagnetic chemical exchange saturation transfer magnetic resonance imaging contrast agent. *Mol Imag* 2012; 11(1): 47–57.
40. Terreno E, Castelli DD, Aime S. Encoding the frequency dependence in MRI contrast media: the emerging class of CEST agents. *Contrast Media Mol Imag* 2010; 5(2): 78–98.
41. Sherry AD, Woods M. Chemical exchange saturation transfer contrast agents for magnetic resonance imaging. *Annu Rev Biomed Eng* 2008; 10: 391–411.
42. Chauvin T, Durand P, Bernier M, Meudal H, Doan B-T, Noury F, Badet B, Beloeil J-C, Tóth É. Detection of enzymatic activity by PARACEST MRI: a general approach to target a large variety of enzymes. *Angew Chem Int Edn* 2008; 47(23): 4370–4372.
43. Schroder L, Lowery TJ, Hilty C, Wemmer DE, Pines A. Molecular imaging using a targeted magnetic resonance hyperpolarized biosensor. *Science* 2006; 314(5798): 446–449.
44. Randtke EA, Chen LQ, Corrales LR, Pagel MD. The Hanes-Woolf linear QUESTP method improves the measurements of fast chemical exchange rates with CEST MRI. *Magn Reson Med*. DOI: 10.1002/mrm.24792.
45. Sun PZ. Simplified quantification of labile proton concentration-weighted chemical exchange rate ( $k(ws)$ ) with RF saturation time dependent ratiometric analysis (QUESTRA): normalization of relaxation and RF irradiation spillover effects for improved quantitative chemical exchange saturation transfer (CEST) MRI. *Magn Reson Med* 2012; 67(4): 936–942.

## SUPPORTING INFORMATION

Additional supporting information may be found in the online version of this article at the publisher's web site.